Hydrothermally-induced melt lens cooling and segmentation along the axis of fast- and intermediate-spreading centers

Fabrice J Fontaine, Jean-Arthur Olive, Mathilde Cannat, Javier Escartin, Thibaut Perol

Hydrothermally-induced melt lens cooling and segmentation along the axis of fast- and intermediate-spreading centers

Fabrice J. Fontaine,[1] Jean-Arthur Olive,[2,3] Mathilde Cannat,[1] Javier Escartin,[1] and Thibaut Perol[2]

Received 14 April 2011; revised 6 June 2011; accepted 11 June 2011; published 28 July 2011.

[1] The heat output and thermal regime of fast and intermediate spreading centers are strongly controlled by boundary layer processes between the hydrothermal system and the underlying crustal magma chamber (AMC), which remain to be fully understood. Here, we model the interactions between a shallow two-dimensional cellular hydrothermal system at temperatures <700°C, and a deeper AMC at temperatures up to 1200°C. We show that hydrothermal cooling can freeze the AMC in years to decades, unless melt injections occur on commensurate timescales. Moreover, the differential cooling between upflow and downflow zones can segment the AMC into mush and melt regions that alternate on sub-kilometric length scales. These predictions are consistent with along-axis variations in AMC roof depth observed in ophiolites and oceanic settings. In this respect, fine-scale geophysical investigations of the structure of AMCs may help constrain hydrothermal recharge locations associated with active hydrothermal sites. **Citation:** Fontaine, F. J., J.-A. Olive, M. Cannat, J. Escartin, and T. Perol (2011), Hydrothermally-induced melt lens cooling and segmentation along the axis of fast- and intermediate-spreading centers, *Geophys. Res. Lett.*, *38*, L14307, doi:10.1029/2011GL047798.

1. Introduction

[2] High-temperature hydrothermal activity along the axis of fast- and most intermediate-spreading mid-ocean ridges is driven by the heat released from a sill-like axial magma chamber (AMC) that appears near-continuous along axis [e.g., *Vera et al.*, 1990; *Van Ark et al.*, 2007] with hydrothermal convection cells that are likely axis-parallel [*Haymon et al.*, 1991; *Coumou et al.*, 2008; *Tolstoy et al.*, 2008]. In contrast, AMCs at slow-spreading ridges are short-lived and discontinuous along axis [*Wilcock and Delaney*, 1996; *Singh et al.*, 2006; *Sinha et al.*, 1997]. Magmatic heat at fast and intermediate spreading ridges is transferred through a thin (10–100 m) thermal boundary layer at the interface between the hydrothermal convection system and the roof of the magma lens [e.g., *Lowell and Germanovich*, 2004]. Understanding the dynamics of this interface is critical, as it controls the thermal regime and hydrothermal (heat and mass) fluxes of about 40% in length of the global mid-ocean ridge system (ridges with spreading rate >56 cm/yr [*Bird*, 2003]), accommodating about 70% of the total release of magmatic heat at mid-ocean ridges [e.g., *Cannat et al.*, 2004].

[3] In the last thirty years, with more detailed and sophisticated geophysical methods, our knowledge of the structure of AMCs has evolved from a geological feature that is continuous along-axis to a complex one, with alternating melt-rich and melt-depleted sections [*Singh et al.*, 1998; *Carton et al.*, 2008]. These data document changes in AMC depth of tens to hundreds of meters on a regional scale of several kilometers to a very few tens of kilometers [*Hooft and Detrick*, 1995; *Singh et al.*, 1998; *Van Ark et al.*, 2007]. New techniques [*Mutter et al.*, 2009] are showing AMC variations in depth at local scale (few tens of m vertically), and in crystallinity on a sub-kilometric scale [*Mutter et al.*, 2010; *Carton et al.*, 2008; *Marjanovic et al.*, 2010]. Further support for local-scale variations may come from ophiolites, where variations of up to 50 m in the AMC depth at spatial scales of 150 to 500 m have been observed [*France et al.*, 2009; *Gillis and Roberts*, 1999].

[4] While the reasons for these complexities are not fully understood, the depth to the AMC roof likely results from a balance between the melt supply to the ridge and its timing, the frequency of volcanic eruptions, and the dynamics of hydrothermal convection. Previous studies discussing this issue have put forward processes able to drain and/or inflate/deflate locally the AMC, linked to variations in melt supply or discharge [e.g., *Carton et al.*, 2008; *France et al.*, 2009]. In this paper, we explore the possible role of hydrothermal activity in AMC cooling and structure. We develop an original two-dimensional numerical model of coupled magmatic and hydrothermal processes that describes the dynamical magmato-hydrothermal interface, and predicts the crystal/melt content of the AMC, as a result of heat mining by hydrothermal convection. The downward migration of the hydrothermal-magmatic interface and its along-axis topography are quantified and discussed in the light of field observations. The amplitude of along-axis variations in AMC crystallinity (melt and mush regions) and the timing of their formation are also investigated. These results constrains the time scales of melt replenishment/supply in the AMC, and are backed up by a first-order analytical model based on a steady-state heat flow balance. Finally, we discuss the relationships between the location of high-temperature seafloor vent fields and the along-axis variations of AMC crystallinity.

2. The Conceptual Model

[5] In Figure 1a we show a classical model of hydrothermal activity tailored for the fast to intermediate ridge

[1]Institut de Physique du Globe de Paris, UMR 7154, CNRS, Sorbonne Paris Cité, Université Denis Diderot Paris 7, Paris, France.
[2]Ecole Normale Supérieure de Paris, UMR 8538, CNRS, Paris, France.
[3]Now at MIT/WHOI Joint Program in Oceanography, Woods Hole, Massachusetts, USA.

0094-8276/11/2011GL047798

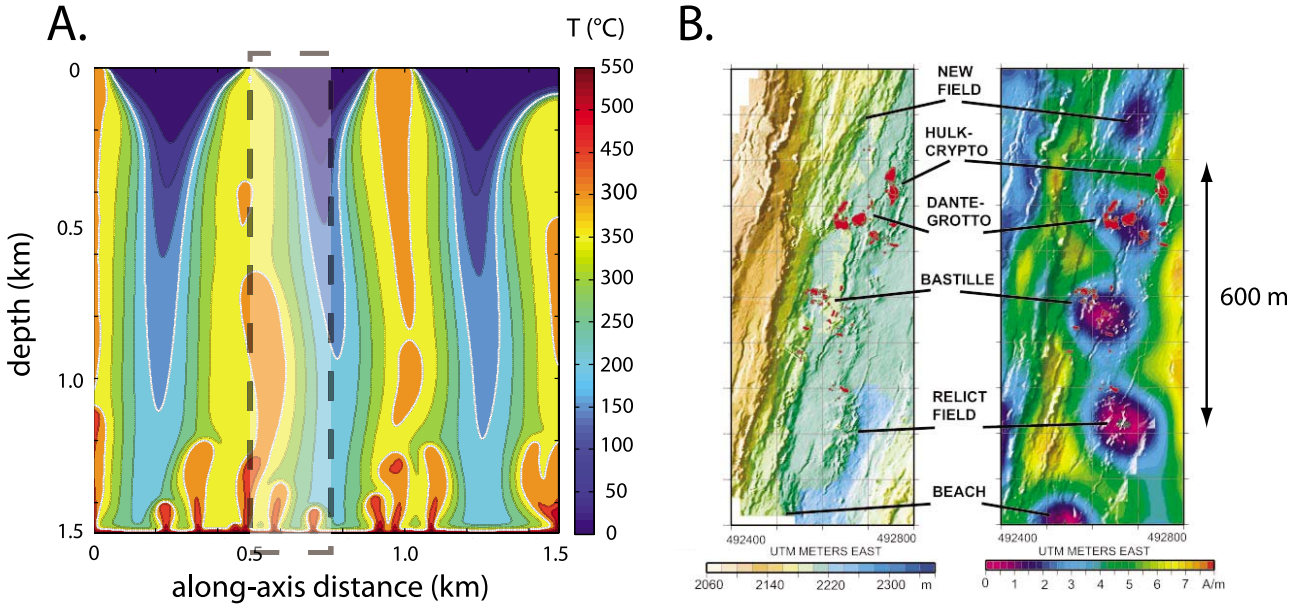

Figure 1. Classical numerical models of cellular hydrothermal circulation at fast to intermediate ridges, and vent distribution at the Main Endeavour Field (MEF). (a) Two-dimensional temperature distribution in a 1.5*1.5 km along-axis vertical crustal cross-section with a permeability of 10^{-14} m^2. The circulation is composed of six similar convective cells producing four, ~100–150 m-wide high-temperature, venting (in yellow-orange) and three, ~350–400-m-wide recharge areas (in blue). White lines represent the 200°C and 400°C isotherms. The dashed box represents the single-cell geometry of the magmato-hydrothermal model presented in this study. (b) Vent site distribution and crustal magnetization at MEF (modified after *Tivey and Johnson* [2002]). Note correlation of ~100 m-wide circular magnetization lows with active and inactive vent areas. The model in Figure 1a could explain the regular vent distribution at MEF, but also at other fields (e.g., Mothra on Juan de Fuca, 9°50N–9°51N at EPR) where vent distribution suggests a periodically organized hydrothermal flow.

environment. Similar convective cells produce focused, evenly distributed venting sites (100–150 m) separated by broader recharge areas (350–400 m). Simple scale analysis [e.g., *Lowell and Germanovich*, 2004] predict this organization: for a uniform permeability system, the number of cells (N) and their size (L) are controlled by the permeability amplitude (k) with $N = \alpha k^{1/2}$, $L = \alpha k^{-1/2}$ and k in the range 10^{-14}–10^{-12} m^2. Such models are invoked to explain the regular distribution of venting areas at several sites along fast and intermediate-spreading ridges, such as the Main Endeavour (Figure 1b) [e.g., *Tivey and Johnson*, 2002; *Coumou et al.*, 2008] and the Mothra [*Kelley et al.*, 2001] fields along the Juan de Fuca ridge, or at 9°50′–51′N on the East Pacific Rise (EPR) [*Fornari et al.*, 2004]. All these sites have typical vent spacing of 50–200 meters. At the EPR between 9°49′N and 9°50′N, a wider, kilometer-long cell has been inferred from microseismicity [*Tolstoy et al.*, 2008], which may be due to a more complex crustal permeability structure [*Crone et al.*, 2011] producing larger convection cells than those shown in Figure 1.

[6] The goal of this work is to study the interactions of these cellular hydrothermal systems with the deeper magmatic layer that fuel them. Because of the periodical nature of the flow, it is reasonable to expect that each of these self-similar hydrothermal cells will interact in the same fashion with the AMC. Accordingly, and in order to limit computation time and increase model resolution, which is critical to describe the thin magmato-hydrothermal boundary, we investigate the interactions of a single, hundreds-of-meter wide two-dimensional hydrothermal cell with the underlying AMC. We discuss the consequences of our model at the local (site) and regional scales.

[7] Our modeling domain is a 3 km deep and 0.375 km long (along-axis) vertical crustal section. The size of the cell produced is thus commensurate with the size of observed and modelled cells at site-scale (Figure 1). This modeling domain is divided into two initially flat layers (Figure 2): a top layer in which hydrothermal processes are modeled at temperatures lower than a given threshold (T_{cut} = 700°C), and a bottom layer at temperatures between T_{cut} and 1200°C, in which magmatic processes are introduced. In the top layer we adopt a classical formalism for high-temperature sub-seafloor hydrothermal convection [*Fontaine and Wilcock*, 2007; *Coumou et al.*, 2008]: open-top simulation domain, darcian flow, energy conservation in a porous medium with an equilibrium temperature ($T_{rock} = T_{fluid}$), and realistic, seawater-based, fluid properties for a single-phase, vapor-like fluid. The bottom layer, being at temperatures >700°C, is in the ductile field [*Hirth et al.*, 1998] and considered impermeable. In this layer, we emplace a magma lens of initial thickness h_{AMC} at depth z_{AMC} in the form of an initially continuous zone of x_c = 0% crystallinity (melt content, x_l = 100%). In this model melt lens, the initial temperature is uniformly 1200°C. Model initial conditions are based on seismic studies at the most magma-rich portions of the EPR, where h_{AMC} = 60 m and z_{AMC} = 1500 m [*Canales et al.*, 2006; *Collier and Singh*, 1997]. We discuss below the effects of deviations from these reference parameters.

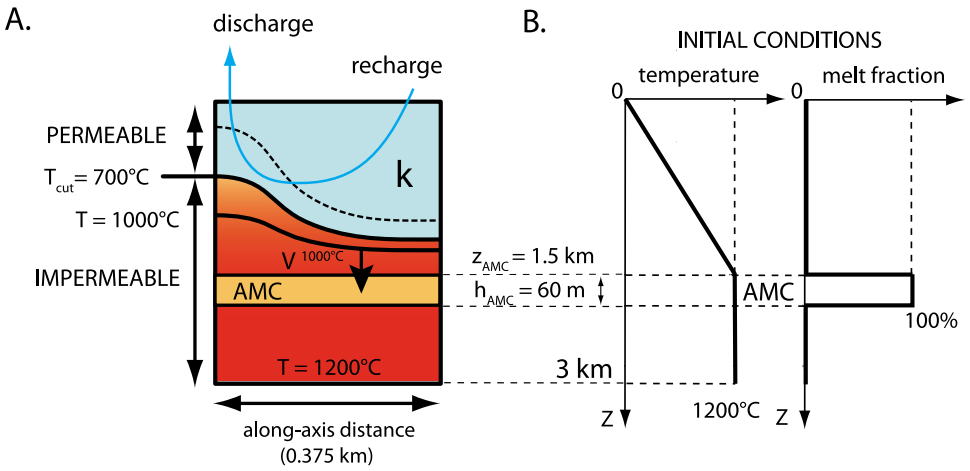

Figure 2. Two-layer conceptual model. (a) The vertical model domain is 3 km-deep and 0.375 km-long, corresponding to inferred depth below seafloor and along-axis length, respectively. Hydrothermal convection is modeled for temperatures lower than 700°C (hydrothermal upper layer). Heat transfers are controlled only by conduction at temperatures between 700°C and 1200°C (magmatic lower layer). Within the 60 m-thick AMC emplaced at 1.5 km depth, latent heat release is taken into account (see Text S1). $V^{1000°C}$: velocity of the downward propagating (black arrow) 1000°C isotherm, k: permeability. (b) Initial conditions are a slightly perturbed linear vertical temperature distribution in the hydrothermal layer and a constant temperature (1200°C) magmatic layer. The melt distribution is 100% in the AMC and zero elsewhere. Flow and energy equations are solved on a 100*800-points grid using a finite differences, implicit alterning direction (ADI), technique described by *Douglas and Rachford* [1956]. Model boundary conditions include impermeable, vertical adiabatic sides, an impermeable base at constant temperature (1200°C at 3 km depth) and an open top (constant pressure of 200 bars and T = 2°C when recharge and $\partial T/\partial z = 0$ when discharge).

[8] As the hydrothermal circulation mines heat from the deeper layer, the AMC cools down and its crystallinity evolves according to a first-order, temperature-dependent law (0% melt at 1000°C, 100% melt at 1200°C) devised by *Sinton and Detrick* [1992] (Text S1 in the auxiliary material).[1] Latent heat released during magma cooling and crystallization is taken into account in our calculations via a modified energy conservation law valid only at temperatures ranging from 1000°C to 1200°C in domains where melt is present (see Text S1). Our "two-layer" approach allows the hydrothermal-magmatic interface, defined as a threshold isotherm (T_{cut}), to move vertically freely in space and time (Figure 2).

3. Results and Physical Discussions

[9] In Figure 3 we show the results of an experiment with a permeability of the hydrothermal layer of 10^{-14} m^2, and which results in geologically realistic heat transported by the model circulation (see section 4 below). After an initial period of 40–50 years required to build the diffusive thermal boundary between the hydrothermal (permeable) and ductile (impermeable) layers, a recharge area forms on one side of the model, while high-temperature fluids (~300°C) upflow and discharge on the other side (Figure 3a). In Figure 3b we show that the formation of recharge and discharge zones leads to a differential cooling of the top of the AMC with recharge extracting more heat than discharge zones. This leads to a "topography" of the "zero-melt front", i.e., the 1000°C isotherm- with a depth difference of 60 m over 375 m laterally between discharge and recharge after 170 years (Figure 3a). Note that these vertical variations are obtained with a solidus temperature (T_S) of 1000°C. A lower T_S would likely increase the amplitude of the topography, as the vertical deflections of the isotherms in the ductile part of the model (T > 700°C) decrease with the distance to the threshold isotherm (T_{cut} = 700°C). Because of this topography, the crystallinity of the AMC increases faster below recharge than below discharge zones (Figures 3c and 3d). Eventually, the AMC is completely crystallized (x_c = 100%) below recharge zones while adjacent AMC sections underlying discharge zones exhibit a melt content x_l > 60–70% (Figure 3d).

[10] For the permeability used in this experiment (k = 10^{-14} m^2), the time required to fully crystallize the AMC below recharge is ~170 years (Figure 3d). We find that both the rate of downward propagation of the zero-melt front, i.e., the 1000°C isotherm, and the AMC crystallization rate, increase linearly when increasing the vigor of the hydrothermal convection, which is controlled by the permeability of the upper layer (Table 1 and Figure S1). This is an expected consequence of the linear relationship between permeability and heat extraction (in W/m^2) detailed in Text S2. These rates are not sensitive to the initial depth of the AMC, and remain in the same orders of magnitude over a realistic range of AMC thicknesses (see Table 1). Our results are consistent with a hydrothermal boundary layer migrating downward into initially impermeable rocks at a constant velocity (proportional to k) while maintaining its thickness (proportional to 1/k; see Text S2).

4. Heat Fluxes

[11] With a permeability of 10^{-14} m^2, we calculate that the mean heat flux at the base of the hydrothermal layer is about 30 W/m^2 (Figure 3b). This model heat flux is comparable to

[1]Auxiliary materials are available in the HTML. doi:10.1029/2011GL047798.

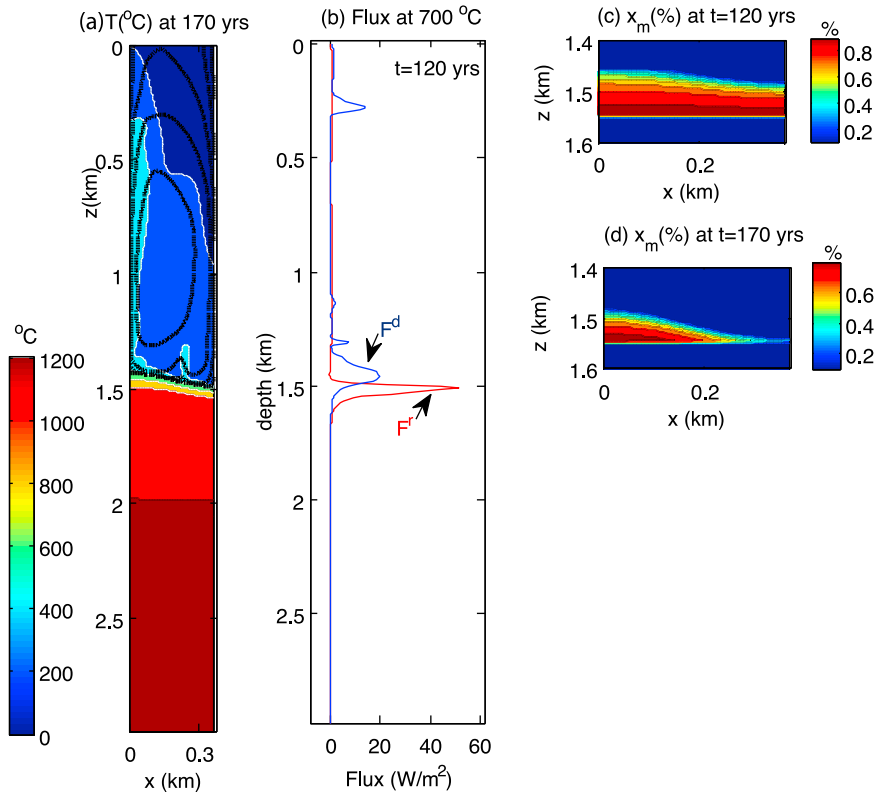

Figure 3. Model results of coupled magmatic and hydrothermal processes. (a) Two-dimensional temperature distribution in a vertical along-axis cross-section of permeability k = 10^{-14} m^2 after a simulation time of 170 years. White lines represent isotherms from 200 to 1000°C and black lines are hydrothermal flow lines. Note that no flow occurs at temperatures >700°C. The thermal boundary layer (isotherms between 600°C and 1000°C) is deeper below recharge than below discharge. (b) Vertical conductive heat flux (in W/m^2) distributions predicted by the model along the right-hand side downflow (red line) and left-hand side upflow (blue line) zones at time 120 years. This heat flux is maximum (F^r and F^d spikes) at the boundary between the lower, ductile and upper, hydrothermal layer (700°C isotherm), where it equals the heat extracted locally by hydrothermal circulation. Heat extraction is enhanced below recharge resulting in the deepening of the isotherms in Figure 3a. (c) Zoom on vertical 2D melt distribution x_m (from 0 to 1) in the AMC at time 120 years. Below recharge, the crystallinity of the AMC increases faster than below discharge because of the higher cooling rate creating a "topography" of the top of the AMC. (d) Same as Figure 3c but at time 170 years. The melt lens is fully crystallized below recharge, while melt content is up to 70% below discharge.

values derived from metamorphic data at the dike-gabbro transition in ophiolites and at fast-spread oceanic settings (e.g., Hess and Pito Deep [*Gillis*, 2008]). Assuming that heat is extracted over a 1 km-wide AMC [*Kent et al.*, 1990] this heat flux would provide about 30 MW per km of ridge, which is within estimates of time-averaged values of heat available per kilometer of ridge axis [*Wilcock and Delaney*, 1996; *Mottl*, 2003; *Cannat et al.*, 2004]. For this hydrothermal configuration, our model predicts the full crystallization of the AMC within a few tens to a few hundreds of years over a realistic range of AMC thicknesses (Table 1).

[12] However, a mean heat flux of 30 MW is one order of magnitude lower than the estimated heat flux at smoker fields such as EPR-9°50′N or Main Endeavour Field (Juan

Table 1. Model Characteristics for Several Simulations With Varying Hydrothermal Layer Permeability[a]

k(m^2)	F^r (W/m^2)	F^d (W/m^2)	$V^{1000°C\|max}$ (m/yr)	dxl/dtl^{max} (% melt/yr)
2.10^{-15}	15	5	0.27	0.18
5.10^{-15}	20,6	12	0.62	0.55
7.10^{-15}	40	15	0.9	0.8
10^{-14}(h_{amc} = 60 m)	55	25	1.4	1.1
10^{-14}(h_{amc} = 120 m)	63	26	1.3	1.2
10^{-14}(z_{amc} = 900 m)	63	28	1.2	1.2

[a]Unless specified, all models are run for AMC depth z_{amc} = 1,5 km and thickness h_{amc} = 60 m. F^r :Maximum spatial and temporal heat flux below recharge- F^d :maximum spatial and temporal heat flux below discharge- $V^{1000°C|max:}$ maximum velocity of the "zero-melt" front, i.e., the 1000°C isotherm- dxl/dtl^{max}: maximum crystallization rate in the AMC, h_{amc}:AMC vertical thickness.

de Fuca Ridge) [e.g., *Lowell and Germanovich*, 2004, and references therein]. This discrepancy could be accounted for in two ways: 1) that these smoker fields mine heat over distances of the order of 10 km or more, as suggested by *German and Lin* [2004] for the Endeavour vents and *VonDamm* [2004] for the EPR vents on the basis of fluid geochemical data; or 2) that upper crustal permeabilities during the formation of these smoker fields are higher than 10^{-14} m^2. The first hypothesis, however, does not account for the distribution of vents observed in the field [e.g., *Kelley et al.*, 2001; *Tivey and Johnson*, 2002; *Tolstoy et al.*, 2008]. In the following discussion, we will investigate the consequences of this second hypothesis.

[13] Given the linear relationships between permeability and heat flux [*Lowell and Germanovich*, 2004] and AMC cooling time (expressed by the velocity of the zero-melt front in Table 1), heat fluxes of hundreds of MW would be consistent with our model's prediction for a permeability of about 10^{-13} m^2 in the hydrothermal layer, which is similar to values that have been predicted in other studies of ridge-axis hydrothermal systems [e.g., *Lowell and Germanovich*, 2004; *Crone et al.*, 2011]. This would cause the AMC to freeze in less than a few years or decades, unless compensated by sustained melt replenishment which seems to be a prerequisite for AMCs to fuel long-lived (>100 years) high-temperature, smoker-like hydrothermal activity as shown by *Liu and Lowell* [2009]. In their recent magmato-hydrothermal models these authors show that freezing of the AMC causes the boundary layer at the base of the system to thicken, leading to a rapid (years to a few decades) decrease of vent temperatures and fluxes. AMC replenishment rates are poorly known, but indirect constraints from geological observations at the EPR support inter-eruption times between a decade and a few hundred years [*Sinton et al.*, 2002; *Rubin and Sinton*, 2007], which could reflect timing of AMC replenishment. Also, the presence of interlayered anorthosite layers, which record the intrusion of new melt within fossil AMCs in the Oman ophiolites, suggests a maximum 100 years periodicity of melt recharge [*Nicolas and Boudier*, 2011]. Our models indicate that such replenishment rates would be adequate to maintain moderate-permeability ($\sim 10^{-14}$–10^{-15} m^2) hydrothermal systems in a quasi steady-state, but too long to invigorate high-permeability systems ($>10^{-13}$ m^2).

[14] As noted above, high permeability, high heat flux hydrothermal systems would extract more heat over a given length of ridge than the time-averaged magmatic heat available for this length of the ridge axis [*Wilcock and Delaney*, 1996; *Mottl*, 2003; *Cannat et al.*, 2004]. Unless heat mining does take place over greater along-axis distances than predicted from the distribution of smoker fields, it follows that these systems should be short-lived, with longer intervening periods of more moderate heat extraction. Such temporal variability would be consistent with a development of vigorous black-smoker type hydrothermal activity linked to magma chamber replenishment episodes. Seismic reflection data by *Singh et al.* [1998] show for example that the AMC crystallinity varies from pure melt to crystal mush along the axis of the southern EPR and that the location of high-temperature vent fields coincides with low crystallinity sections of the AMC. Based on interpretations of focal mechanisms at Endeavour (Juan de Fuca ridge), *Wilcock et al.* [2009] complement this idea and infer that on-going replenishment of the AMC and emplacement of pressurized magma induce stress perturbations that enhance the permeability of the hydrothermal layer.

5. AMC Segmentation

[15] The seismic observations by *Singh et al.* [1998] indicate that well crystallized AMC sections about 20 km-long represent 80% of the length of the EPR between latitudes 14°S and 14°30′S. Although these mushy, high-temperature (>1000°C) AMC sections are found at a similar depth than the adjacent melt-rich sections, they do not seem to fuel high-temperature hydrothermal activity at the seafloor [*Singh et al.*, 1998]. In the light of our model, this could be explained in two ways: 1) that subcritical (in regard to hydrothermal convection) permeabilities ($<10^{-16}$ m^2) characterize the axial lithosphere above high crystallinity AMC sections, or 2) that crustal permeability above the mushy sections is moderate ($\sim 10^{-14}$–10^{-15} m^2) and comparable to values used in our model (Figure 3), but that high- temperature fluids do not make it to the seafloor because of fluid-rock interactions (e.g., mineral precipitation [*Fontaine et al.*, 2001]), mixing and cooling of hydrothermal fluids along the volcanic sections, and/or permeability structure [e.g., *Wilcock*, 1998]. In this latter case, the hydrothermal circulation will mine heat from the AMC and either replenishment rates commensurate to the AMC cooling rates reproduced in our models are required to ensure steady-state, or the magmato-hydrothermal transition will propagate downward as described by *Gillis* [2008]. In this respect, it is worth noting that our model considers a uniform permeability hydrothermal layer. Permeability contrasts between upflow and downflow zones are poorly constrained, but a higher recharge than discharge permeability due to mineral precipitation/dissolution (e.g., anhydrite or sulphurs [*Lowell et al.*, 2003; *Fontaine et al.*, 2001]) will proportionally decrease AMC cooling time, and vice-versa.

[16] Our model also predicts that the differential hydrothermal cooling between recharge and discharge zones could produce variations in the topography of the AMC roof (1000°C isotherm in Figure 3a) and its crystallinity at scales of a few hundred meters. The time period of these short-wavelength variations would be conditioned by the permeability in the hydrothermal domain (1–10 years timescale with a $k = 10^{-13}$ m^2, and one order of magnitude longer timescale for $k = 10^{-14}$ m^2). The spatial scale of these short-wavelength variations is controlled by the hydrothermal cell geometry, which is in turn controlled by the crustal permeability structure (amplitude, anisotropy) and which remains poorly constrained in nature. If zones of upflow likely match zones of venting on the seafloor, the location and size of recharge areas remain highly hypothetical and site-dependent. Accordingly, local, sub-kilometer-scale geophysical investigations (e.g., seismic, electro-magnetic) of the structure of AMC (depth, crystallinity) at active, high-temperature vent fields may help constrain hydrothermal recharge locations.

[17] At the Main Endeavour (Figure 1b), Mothra, and 9°50–9°51N fields, where recharge is thought to occur between the regularly spaced venting areas, our results suggest that the underlying AMC could be hydrothermally segmented into regularly-spaced mush (below recharge) and melt (below discharge) regions. At 9°49N, the AMC discontinuity below the downflow limb of the km-wide hydrothermal cell [*Tolstoy et al.*, 2008], and the along-axis variations in the AMC

reflector depth [*Mutter et al.*, 2010; *Marjanovic et al.*, 2010] and in its crystallinity [*Carton et al.*, 2008], could also result from differential hydrothermal cooling, Finally, although exceptional, the short wavelength spatial variations in AMC depth observed in ophiolites (50 m vertical offset for 150 m along axis [*France et al.*, 2009]), may also result from hydrothermal cooling.

6. Conclusions

[18] In this work we show that the continuous axial melt lenses (AMC) underlying fast and most intermediate-spreading ridges should be cooled by hydrothermal circulation in a few years to a few hundreds of years depending on the permeability of the upper axial crust. For high-permeability configurations, high heat flux systems such as those discovered along the East Pacific Rise at 9°50′N and Endeavour segment on Juan de Fuca would form and freeze the AMC below in a few years unless replenished on a commensurate time scale. For moderate permeability configurations, an AMC could be maintained with lower replenishment rates (a few hundreds of years). Our results are in agreement with, and complement the analytical approach of *Liu and Lowell* [2009], bringing constraints on the cooling geometry at the magmato-hydrothermal interface. Our models also predict that hydrothermal activity is able to produce along-axis variations of the depth and crystallinity of the AMC that is controlled by hydrothermal cell size, with melt-rich (below hydrothermal discharge) and melt-depleted (below hydrothermal recharge) zones. In our models, this segmentation is produced over timescales of a few years to tens of years, this duration being linearly related to permeability in the hydrothermal domain. Sites such as EPR-9°50′N (fast-spreading) or Main Endeavour Field, Juan de Fuca ridge (intermediate spreading) where hydrothermal flow is thought to occur dominantly along axis [*Tolstoy et al.*, 2008; *Kelley et al.*, 2001], may be the locus of such hydrothermally-induced short-scale (a few hundred meters along axis) AMC segmentation. This hydrothermally-induced segmentation hypothesis represents an alternative to eruption-controlled models to explain short-scale crystallinity variations and discontinuities in AMC. We propose that, in nature, it is likely that both processes can contribute to AMC segmentation.

[19] **Acknowledgments.** The authors thank Michel Rabinowicz for helpful discussions on early versions of the manuscript. This is Institut de Physique du Globe de Paris contribution 3183.

[20] The Editor thanks Kathryn M. Gillis and W. Buck for their assistance in evaluating this paper.

References

Bird, P. (2003), An updated digital model of plate boundaries, *Geochem. Geophys. Geosyst.*, *4*(3), 1027, doi:10.1029/2001GC000252.

Canales, J. P., S. C. Singh, R. S. Detrick, S. M. Carbotte, A. J. Harding, G. M. Kent, J. P. Diebold, and M. R. Nedimovic (2006), Seismic evidence for variation in axial magma chamber properties along the southern Juan de Fuca Ridge, *Earth Planet. Sci. Lett.*, *246*, 353–366, doi:10.1016/j.epsl.2006.04.032.

Cannat, M., J. Cann, and J. Mclennann (2004), Some hard rock constraints on the supply of heat to mid-ocean ridges, in *Mid-Ocean Ridges: Hydrothermal Interactions Between the Lithosphere and Oceans*, *Geophys. Monogr. Ser.*, vol. 148, edited by C. R. German et al., pp. 111–149, AGU, Washington, D. C.

Carton, H., et al. (2008), Characteristics of the crustal magma body in the 2005–06 eruption area at 9°50′N on the East Pacific Rise from a 3D multi-channel seismic investigation, Abstract B23F-03 presented at 2010 Fall Meeting, AGU, San Francisco, Calif., 13–17 Dec.

Collier, J. S., and S. C. Singh (1997), Detailed structure of the top of the melt body beneath the East Pacific Rise at 9°40′N from waveform inversion of seismic reflection data, *J. Geophys. Res.*, *102*, 20,287–20,304, doi:10.1029/97JB01514.

Coumou, D., T. Driesner, and C. A. Heinrich (2008), The structure and dynamics of mid-ocean ridge hydrothermal systems, *Science*, *321*, 1825–1828, doi:10.1126/science.1159582.

Crone, T. J., M. Tolstoy, and D. F. Stroup (2011), Permeability structure of young ocean crust from poroelastically triggered earthquakes, *Geophys. Res. Lett.*, *38*, L05305, doi:10.1029/2011GL046820.

Douglas, J., and H. H. Rachford (1956), On the numerical solution of heat conduction problems in two and three space variables, *Trans. Am. Math. Soc.*, *82*, 421–439, doi:10.1090/S0002-9947-1956-0084194-4.

Fontaine, F., and W. Wilcock (2007), Two dimensional models of hydrothermal convection at high Rayleigh and Nusselt numbers: Implications for mid-ocean ridges, *Geochem. Geophys. Geosyst.*, *8*, Q07010, doi:10.1029/2007GC001601.

Fontaine, F., M. Rabinowicz, and J. Boulègue (2001), Permeability changes due to mineral diagenesis in fractured crust: Implications for hydrothermal circulation at mid-ocean ridges, *Earth Planet. Sci. Lett.*, *184*, 407–425, doi:10.1016/S0012-821X(00)00332-0.

Fornari, D., et al. (2004), Submarine lava flow emplacement at the East Pacific Rise 9°50′N: Implications for uppermost crust stratigraphy and hydrothermal fluid circulation, in *Mid-Ocean Ridges: Hydrothermal Interactions Between the Lithosphere and Oceans*, *Geophys. Monogr. Ser.*, vol. 148, edited by C. R. German et al., pp. 187–217, AGU, Washington, D. C.

France, L., B. Ildefonse, and J. Koepke (2009), Interactions between magma and hydrothermal system in Oman ophiolite and in IODP Hole 1256D: Fossilization of a dynamic melt lens at fast spreading ridges, *Geochem. Geophys. Geosyst.*, *10*, Q10O19, doi:10.1029/2009GC002652.

Gillis, K. M. (2008), The roof of an axial magma chamber: A hornfelsic heat exchanger, *Geology*, *36*, 299–302, doi:10.1130/G24590A.1.

Gillis, K. M., and M. Roberts (1999), Cracking at the magma-hydrothermal transition: Evidence from the Troodos ophiolite, *Earth Planet. Sci. Lett.*, *169*, 227–244, doi:10.1016/S0012-821X(99)00087-4.

Haymon, R. M., et al. (1991), Hydrothermal vent distribution along the East Pacific Rise crest (9°09′–54′N) and its relationship to magmatic and tectonic processes on fast-spreading mid-ocean ridges, *Earth Planet. Sci. Lett.*, *104*, 513–534, doi:10.1016/0012-821X(91)90226-8.

Hirth, G., J. Escartin, and J. Lin (1998), The rheology of the lower oceanic crust: Implications for lithospheric deformation at mid-ocean ridges, in *Faulting and Magmatism at Mid-Ocean Ridges*, *Geophys. Monogr. Ser.*, vol. 106, edited by W. R. Buck et al., pp. 291–303, AGU, Washington, D. C.

Hooft, E. E. E., and R. S. Detrick (1995), Relationship between axial morphology, crustal thickness, and mantle temperature along the Juan de Fuca and Gorda ridges, *J. Geophys. Res.*, *100*, 22,499–22,508, doi:10.1029/95JB02502.

Kelley, D. S., J. R. Delaney, and D. R. Yoerger (2001), Geology and venting characteristics of the Mothra hydrothermal field, Endeavour segment, Juan de Fuca Ridge, *Geology*, *29*, 959–962, doi:10.1130/0091-7613(2001)029<0959:GAVCOT>2.0.CO;2.

Kent, G. M., A. J. Harding, and J. A. Orcutt (1990), Evidence for a small magma chamber beneath the East Pacific Rise at 9°30 N, *Nature*, *344*, 650–653, doi:10.1038/344650a0.

Lapwood, E. R. (1948), Convection of a fluid in a porous medium, *Proc. Cambridge Philos. Soc.*, *44*, 508–521, doi:10.1017/S030500410002452X.

Liu, L., and R. P. Lowell (2009), Models of hydrothermal heat output from a convecting, crystallizing, replenished magma chamber beneath an oceanic spreading center, *J. Geophys. Res.*, *114*, B02102, doi:10.1029/2008JB005846.

Lowell, R. P., and D. K. Burnell (1991), A numerical model for magma-hydrothermal boundary layer heat transfer in the oceanic crust, *Earth Planet. Sci. Lett.*, *104*, 59–69, doi:10.1016/0012-821X(91)90237-C.

Lowell, R. P., and L. N. Germanovich (2004), Hydrothermal processes at mid-ocean ridges: Results from scale analysis and single-pass models, in *Mid-Ocean Ridges: Hydrothermal Interactions Between the Lithosphere and Oceans*, *Geophys. Monogr. Ser.*, vol. 148, edited by C. R. German et al., pp. 219–244, AGU, Washington, D. C.

Lowell, R., Y. Yao, and L. Germanovich (2003), Anhydrite precipitation and the relationship between focused and diffuse flow in seafloor hydrothermal systems, *J. Geophys. Res.*, *108*(B9), 2424, doi:10.1029/2002JB002371.

Marjanovic, M., et al. (2010), Axial magma chamber segmentation along the East Pacific Rise from Clipperton to Siqieros Fracture Zone, Abstract OS21C-1511 presented at 2010 Fall Meeting, AGU, San Francisco, Calif., 13–17 Dec.

Mottl, M. J. (2003), Partitioning of energy and mass fluxes between mid-ocean ridge axes and flanks at high and low temperature, in *Energy and Mass Transfer in Marine Hydrothermal Systems*, edited by P. E. Halbach et al., pp. 271–286, Dahlem Univ. Press, Berlin.

Mutter, J. C., S. Carbotte, M. Nedimovic, J. P. Canales, and H. Carton (2009), Seismic imaging in three dimensions on the East Pacific Rise, *Eos Trans. AGU*, *90*(42), doi:10.1029/2009EO420002.

Mutter, J. C., et al. (2010), Eruption-related changes in magma chamber structure at 9° 50′N on the EPR from coincident reflection images, 1985 and 2008, Abstract OS241-01 presented at 2010 Fall Meeting, AGU, San Francisco, Calif., 13–17 Dec.

Nicolas, A., and F. Boudier (2011), Structure and dynamics of ridge axial melt lenses in the Oman ophiolite, *J. Geophys. Res.*, *116*, B03103, doi:10.1029/2010JB007934.

Nield, D. A., and A. Bejan (1992), *Convection in Porous Media*, Springer, New York.

Rubin, K. H., and J. M. Sinton (2007), Inferences on mid-ocean ridge thermal and magmatic structure from MORB compositions, *Earth Planet. Sci. Lett.*, *260*, 257–276, doi:10.1016/j.epsl.2007.05.035.

Singh, S. C., G. M. Kent, J. S. Collier, A. J. Harding, and J. A. Orcutt (1998), Melt to mush variations in crustal magma chamber properties along the ridge crest at the southern East Pacific Rise, *Nature*, *394*, 874–878, doi:10.1038/29740.

Singh, S. C., W. C. Crawford, H. Carton, T. Seher, V. Combier, M. Cannat, J. P. Canales, D. Düsünur, J. Escartín, and J. Miranda (2006), Discovery of a magma chamber and faults beneath a Mid-Atlantic Ridge hydrothermal field, *Nature*, *442*, 1029–1032, doi:10.1038/nature05105.

Sinha, M. C., D. A. Navin, L. M. MacGregor, S. C. Constable, C. Peirce, A. White, G. Heinson, and M. A. Inglis (1997), Evidence for accumulated melt beneath the slow-spreading Mid-Atlantic Ridge, *Philos. Trans. R. Soc. A*, *355*, 233–253, doi:10.1098/rsta.1997.0008.

Sinton, J. M., and R. S. Detrick (1992), Mid-ocean ridge magma chambers, *J. Geophys. Res.*, *97*, 197–216, doi:10.1029/91JB02508.

Sinton, J., E. Bergmanis, K. Rubin, R. Batiza, T. K. P. Gregg, K. Grönvold, K. C. Macdonald, and S. M. White (2002), Volcanic eruptions on mid-ocean ridges: New evidence from the superfast spreading East Pacific Rise, 17°–19°S, *J. Geophys. Res.*, *107*(B6), 2115, doi:10.1029/2000JB000090.

Tivey, M. A., and H. P. Johnson (2002), Crustal magnetization reveals subsurface structure of Juan de Fuca Ridge hydrothermal vent fields, *Geology*, *30*, 979–982, doi:10.1130/0091-7613(2002)030<0979:CMRSSO>2.0.CO;2.

Tolstoy, M., F. Waldhauser, D. R. Bohnenstiehl, R. T. Weekly, and W.-Y. Kim (2008), Seismic identification of along-axis hydrothermal flow on the East Pacific Rise, *Nature*, *451*, 181–184, doi:10.1038/nature06424.

Van Ark, E. M., R. S. Detrick, J. P. Canales, S. M. Carbotte, A. J. Harding, G. M. Kent, M. R. Nedimovic, W. S. D. Wilcock, J. B. Diebold, and J. M. Babcock (2007), Seismic structure of the Endeavour Segment, Juan de Fuca Ridge: Correlations with seismicity and hydrothermal activity, *J. Geophys. Res.*, *112*, B02401, doi:10.1029/2005JB004210.

Vera, E. E., J. C. Mutter, J. A. Orcutt, A. J. Harding, M. E. Kappus, R. S. Detrick, and T. M. Brocher (1990), The structure of 0- to 0.2-m.y.-old oceanic crust at 9°N on the East Pacific Rise from expanded spread profiles, *J. Geophys. Res.*, *95*, 15,529–15,556, doi:10.1029/JB095iB10p15529.

Wilcock, W. S. D. (1998), Cellular convection models of mid-ocean ridge hydrothermal circulation and the temperatures of black smoker fluids, *J. Geophys. Res.*, *103*, 2585–2596, doi:10.1029/97JB03252.

Wilcock, W. S. D., and J. R. Delaney (1996), The size of mid-ocean ridge sulfide deposits: Evidence for heat extraction from magma chambers or cracking fronts, *Earth Planet. Sci. Lett.*, *145*, 49–64, doi:10.1016/S0012-821X(96)00195-1.

Wilcock, W. S. D., E. E. E. Hooft, D. R. Toomey, P. R. McGill, A. H. Barclay, D. S. Stakes, and T. M. Ramirez (2009), The role of magma injection in localizing black-smoker activity, *Nat. Geosci.*, *2*, 509–513, doi:10.1038/ngeo550.

M. Cannat, J. Escartin, and F. J. Fontaine, Institut de Physique du Globe de Paris, UMR 7154, CNRS, Sorbonne Paris Cité, Université Denis Diderot Paris 7, 1 rue Jussieu, F-75238 Paris CEDEX 05, France. (fontaine@ipgp.fr)

J.-A. Olive, MIT/WHOI Joint Program in Oceanography, 360 Woods Hole Rd., Woods Hole, MA 02543, USA.

T. Perol, Ecole Normale Supérieure de Paris, UMR 8538, CNRS, 24 rue Lhomond, F-75231 Paris CEDEX 05, France.